Available online at https://link.springer.com/journal/42241
http://www.jhydrodynamics.com
Journal of Hydrodynamics, 2022, 34(1): 106-115
https://doi.org/10.1007/s42241-022-0011-x

Numerical study of free end effect of cylinder with low aspect ratios on vortex induced motion

Jia-wei He[1], Wei-wen Zhao[1], De-cheng Wan[1, 2*], Yi-qian Wang[3]
1. *Computational Marine Hydrodynamics Lab (CMHL), School of Naval Architecture, Ocean and Civil Engineering, Shanghai Jiao Tong University, Shanghai 200240, China*
2. *Ocean College, Zhejiang University, Zhoushan 316021, China*
3. *School of Mathematical Science, Soochow University, Suzhou 215006, China*

(Received November 22, 2021, Revised January 25, 2022, Accepted January 26, 2022, Published online February 25, 2022)

Abstract: In this paper, numerical simulation is conducted via our in-house solver, vim-FOAM-SJTU, developed on open-source software, OpenFOAM. Flow around static rigid cylinders and elastically mounted rigid cylinder constrained to free stream with free end are numerically investigated. Some significant conclusions are made by analyzing the different results between cases with and without free end. The turbulence model is implemented with a shear stress transport-based (SST-based) improved delayed detached eddy simulation (IDDES) approach in the vim-FOAM-SJTU. Firstly, The paper starts with the application of the vim-FOAM-SJTU solver to flow past fixed cylinder with free end at Reynolds number 43 000. The numerical results are compared with experimental data. Comparison are satisfactory which implies the validity and accuracy of the current computational fluid dynamics (CFD) solver. The flow visualization in the vicinity of free-end is discussed. Subsequently, the solver is utilized to simulate the free end effect associated with the VIM of a cylinder submerged in current. The motion responses under different inflow velocities are studied. The relationship between transverse motion frequency, in-line motion frequency is discussed. Lastly, the effect of the free end on the vortex of the wake field is analyzed by comparing the 3-D vorticity diagrams of the free end cylinder. The responses of circular cylinder with or without free end are compared.

Key words: Fluid-structure interaction, vim-FOAM-SJTU solver, vortex induced motion (VIM), Three-dimensional character

Introduction

With the exploration of offshore oil and renewable energy utilization, the deep-sea floating offshore platforms gain much attention in the industry. However, one of the most challenging issues for floating offshore platforms is the vortex-induced motions (VIM). As floating offshore platform contains column with large aspect ratio, it is subject to large amplitude motions under certain sea conditions, due to periodic pressure change caused by the alternative vortex shedding of columns. A clear understanding of the mechanism of VIM is essential to the security of floating platforms.

Investigations of the flow around cylinder structures have been conducted by many researchers. Recent experimental studies[1-4] as well as recent numerical simulations[5-12], have led to an improved physical understanding of the near-wake vortex flow patterns. Sumner and Heseltine[13] pointed out the tip vortex structure for a circular cylinder with a free end is distinctly different from the infinite cylinders. For a cylinder with free end, Gonçalves et al.[1] reported that the overall drag force coefficients decrease as the aspect ratio deceased, and also reported a decrease in Strouhal number. The overall drag is still smaller than that of an infinitely long cylinder without free end.

Floaters have cylindrical hull bodies such as spars or multiple columns such as semi-submersibles and tension-leg platforms (TLP). Therefore, the flow around a cylinder is usually studied in the VIM context. There are many influence factors of VIM, which makes itself a very complicated problem. The dimension, geometric arrangement of the platform, draft condition, current velocity are key factors found to

Project supported by the National Natural Science Foundation of China (Grant Nos. 52131102, 51909160 and 51879159), the National Key Research and Development Program of China (Grant No. 2019YFB1704200).
Biography: Jia-wei He (1992-), Male, Ph. D. Candidate,
E-mail: jiaweihe@sjtu.edu.cn
Corresponding author: De-cheng Wan,
E-mail: dcwan@sjtu.edu.cn

trigger VIM. The researchers[14–18] reported a good oversight on the VIM of offshore platform. In brief, major concerns of VIM often focus on the surge and sway motion of platforms. For the numerical studies on the vortex induced motion of a cylinder, most of studies in literature are focused on 2-D simulations. Hirabayashi[19] numerically simulated the vortex-induced motion of 2-D circular cylinder by lattice Boltzmann method at low Reynolds number ($Re = 500$). Duranay and Kinaci[20] proposed a numerical approach to include three-dimensionality effects to enhance 2-D numerical flow solutions in vortex-induced vibrations.

However, the flow in the vicinity of the free end of finite circular cylinder, and its relationship to near wake, has not been systematically studied. The effects of free end on the vortex induced motion to cylinder are also not completely understood. Motivated by this, in this study, a three-dimensional numerical study was adopted to investigate free end effect of cylinder undergoing vortex induced motion. The present work is a part of numerical effort to comprehensively investigate VIM response of floating platform.

The current paper reports some of our recent findings regarding the free end effect associated with the VIM of a cylinder submerged in current. We mainly focus on three aspects. Firstly, the accuracy and capability of vim-FOAM-SJTU in study of vortex induced motion of cylinder in current at subcritical Reynolds number. Next, the effect of the free end on the vortex of the wake field is analyzed by comparing the three-dimensional vorticity diagrams of the free end cylinder. The last part shows the results related to vortex induced motion of the free-end cylinder at different reduced velocities. It is anticipated that the current paper would bring deep insights into the intriguing features involved in cylinders' VIM.

1. Numerical method

1.1 *Governing equations*

It is assumed that the fluid is Newtonian and viscous incompressible. The complexity of flow fields over cylinder is obtained by solving the full Navier-Stokes equations taking account the VIM of the cylinder and its interaction with the surrounding fluid. For incompressible viscous fluids, the continuity equation and momentum equation can be expressed as:

$$\frac{\partial \rho u}{\partial t} + \boldsymbol{u} \cdot \nabla \rho \boldsymbol{u} = -\nabla p + \nabla \cdot (\mu \nabla \boldsymbol{u}) + \boldsymbol{f} \tag{1}$$

$$\nabla \cdot \boldsymbol{u} = 0 \tag{2}$$

where $\boldsymbol{u}$ denotes the velocity vector, ρ is fluid density, p is the pressure, μ is the dynamic viscosity of fluid and $\boldsymbol{f}$ is the body force.

The six-degree-of-freedom (DOF) rigid-body equations of motion with linear springs in the Cartesian coordinate is expressed as

$$m\ddot{\boldsymbol{r}} + c\dot{\boldsymbol{r}} + k\boldsymbol{r} = \boldsymbol{F} \tag{3}$$

where m is the mass of cylinder, $\boldsymbol{r}$, $\dot{\boldsymbol{r}}$ and $\ddot{\boldsymbol{r}}$ is the displacement, velocity, and acceleration tensors of the cylidner, respectively, c is the damping of sys-term, k is the spring stiffness and $\boldsymbol{F}$ is the fluid forces acting on the cylidner.

In this paper, the governing equations are discretized using the finite volume method. The time discretization is done using second order implicit backward scheme. The convection term is discretized using (LUST) scheme. A second order Gauss integration is used for diffusion term. The hybrid PISO-SIMPLE (PIMPLE) algorithm is used for solving the coupled pressure-velocity equations. The validation of the solver to simulate a semi-submersible on model scale have been done[21].

1.2 *Turbulence model*

In order to predict VIM responses of the cylinder accurately, a improved delayed detached eddy simulation (IDDES) method based on the shear stress transport (SST) model is used to simulate the turbulence detached flow during a large range of high Reynolds numbers. SST-IDDES is a hybrid Reynolds averaged Navier-Stokes (RANS), large eddy simulation (LES) method. It utilizes sub-grid scale model to handle the flow in the free shear flow area far away from wall, and employs RANS's SST model to solve the flow in the boundary layer near wall and other areas. This can guarantee the accuracy of LES solution, and reduce the amount of calculation in the near-wall region of the boundary layer. The turbulence model applied to the calculations was the SST-IDDES. The SST-IDDES was presented as an improvement of the SST-DDES in Ref. [22].

2. Case setup and the meshes

2.1 *Computational domain and grids*

The computational model in this paper is the same as the model of experiment by Gonçalves et al.[23]. The model of the cylinder and detail parameters are shown in Table 1.

The numerical domain and boudary conditions are shown in Fig. 1. For the case of cylinder with free end, the length of the entire computational domain is $20D$, the width is $10D$ and the height is $5.68D$.

Table 1 Main parameters of the computational model

Description	Value
Cylinder diameter, D /m	0.125
Draft, L /m	0.25
Mass, M /kg	3.068
Vertical center of gravity position, KG /m	0.0577
Metacentric height, GM /m	0.0712

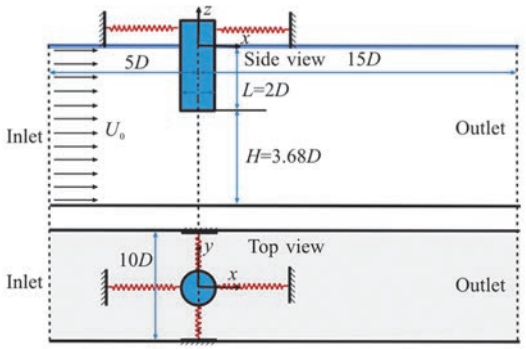

Fig. 1 (Color online) Numerical setup and main dimensional parameters of cylinder with free end

The boundary conditions of the computational domain are set as follow: Free stream velocity for inlet, pressure equals zero for outlet, symmetry for top, the rest of the boundaries is defined as symmetry boundary.

To perform this analysis, meshes with domain O-type were developed and for each domain type were created three levels of refinement with quadrilateral elements. The details of the grids are shown in Fig. 2, yielding a total of 3.52×10^6 grid points for the case of cylinder with free end. Around the cylinder $2.5D$ regions refinement grid cells is used in lateral and streamwise direction whose function is to capture more detailed flow characteristics. A very fine grid near the free-end region. The first layer length is $0.0002\,D$, corresponding to approximately $y^+ = 5$.

The time step is 0.01 s in each case. The workload is distributed into 56 processors on a Linux cluster for calculation.

2.2 *The simulation cases*

Table 2 presents the simulation cases of present study. Because of the speed of incoming current are reasonably not high enough, so that the free surface effect could be ignored[24], correspondingly, the free surface was treated as a symmetric boundary in present numerical simulation. As Goncalves and Fujarra[25] pointed out that the difference of VIM motion amplitude between 2DOF, 6DOF is minimal. Therefore, the numerical simulation of cylindrical vortex induced motion in this paper focuses on two main direction, which is the transverse and in-line motion. The speed of incoming current is vary from 0.075 m/s to 0.175 m/s. The Reynolds numbers involved are between 0.625×10^4, 2.188×10^4.

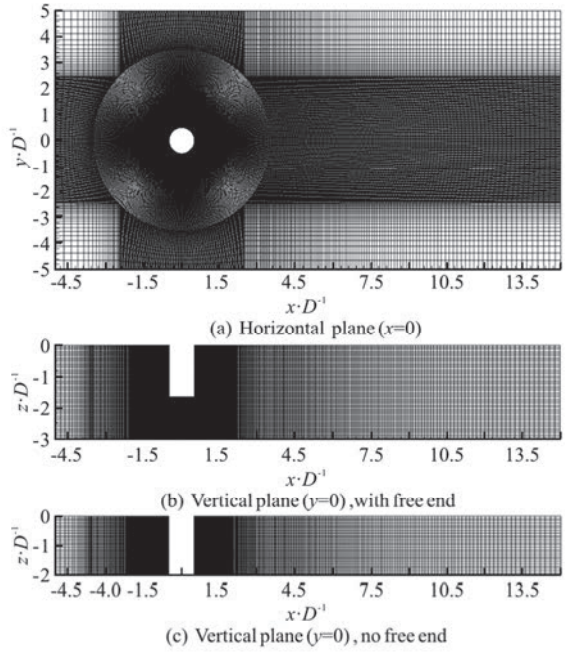

Fig. 2 Details of the mesh around cylinder

Table 2 CFD simulation case conditions of VIM

Cases	Reduced velocity, U_r	Flow velocity/(m·s^{-1})	Re
A	6	0.075	0.938×10^4
B	8	0.100	1.250×10^4
C	10	0.125	1.563×10^4
D	12	0.150	1.875×10^4
E	15	0.175	2.188×10^4

Here, the reduced velocity (U_r) is normally defined as

$$U_r = \frac{U}{f_n D} \tag{4}$$

where U is the velocity of incoming current, f_n is the natural frequency of the cylinder and D is the diameter of the cylinder.

3. Results and discussions

3.1 *The flow around fixed cylinder with free end*

It was firstly performed numerical simulation for a flow around a stationary cylinder, this is, in a zero DOF conformation. The obtained results were com-

pared with the data described in the literature so the vim-FOAM-SJTU solver as well as the obtained results could be validated. Figure 3 shows the comparison of the average drag coefficient $\overline{C_d}$ in this work as well as in previous numerical calculations by Iungo et al.[3], Rosetti et al.[26], and Schlichting and Shapiro[27] for the cylinder without free ends. At this point, it was also studied how the free end could influence the obtained numerical results of flow around cylinder.

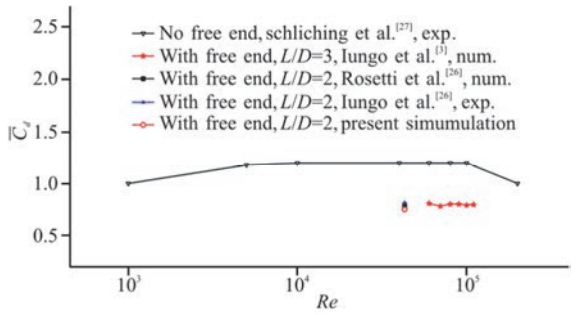

Fig. 3 (Color online) The average drag coefficients from numerical calculations and experiments

As can be observed in Table 3, Fig. 4, the average drag coefficient C_d decreases from 0.99 to 0.71. For the cylinder without free ends, the Stanton number is 0.20, while the value of St is 0.12 for with free end case. The time history curve of the lift coefficient can be seen to fluctuate above and below the value of 0, except that the fluctuation amplitude of the model without the free end is slightly larger than that of the model with the free end. It can be seen that the presence of the free end makes the vortex have multiple frequency components, and there is no longer a single distinct main frequency as in the case of the cylinder without the free end.

Table 3 Comparison of the calculated results with or without free end

Item	Re	$\overline{C_d}$	$C_{l\text{-rms}}$	St
With free end	43 000	0.71	0.05	0.12
No free end	43 000	0.99	0.13	0.20

The velocity field near to the fixed cylinder is shown in Fig. 5. The flow velocity in the near flow field behind the cylinder is larger than that in the far flow field. Overall, for the case of cylinder with free end, the flow velocity is larger than that of cylinder without free end. The length of the wake field zone with the free-ended cylinder is longer than that of cylinder without free end, and it is analyzed that the tip vortex of the free-ended cylinder consumes most of the energy.

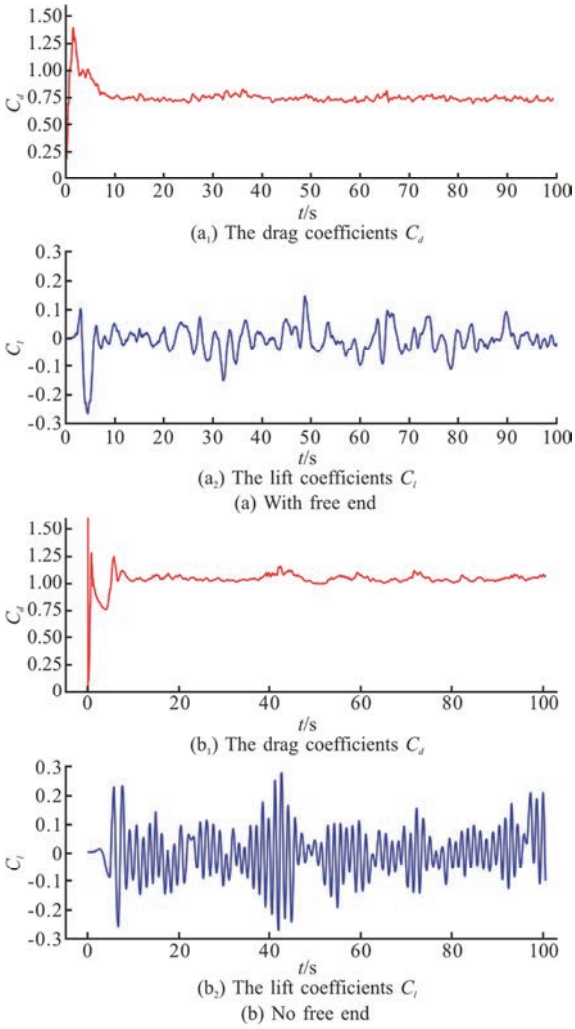

Fig. 4 (Color online) Time-dependent lift and drag coefficients on the circular cylinder (Re = 43 000)

The 3-D vortex contour of flow around fixed cylinder is shown in Fig. 6. For the flow around cylinder with a free-end, it is obvious that a tip vortex is generated from the free end. What's more, a "horseshoe-shaped" vortex appears in the flow field in front of the cylinder near the fixed wall.

3.2 *The free decay test before VIM simulation*

The free decay tests in calm water were conducted to confirm the accuracy of the simplified spring system before the VIM simulation. In the numerical simulation of free decay test, the cylinder is placed to about $0.25D$ away from the x-axis and released with an initial velocity of 0.1 m/s in the absence of incoming flow.

The cylinder will undergo free decay motion under the mooring system, and the calculated results of natural periods are shown in Fig. 7.

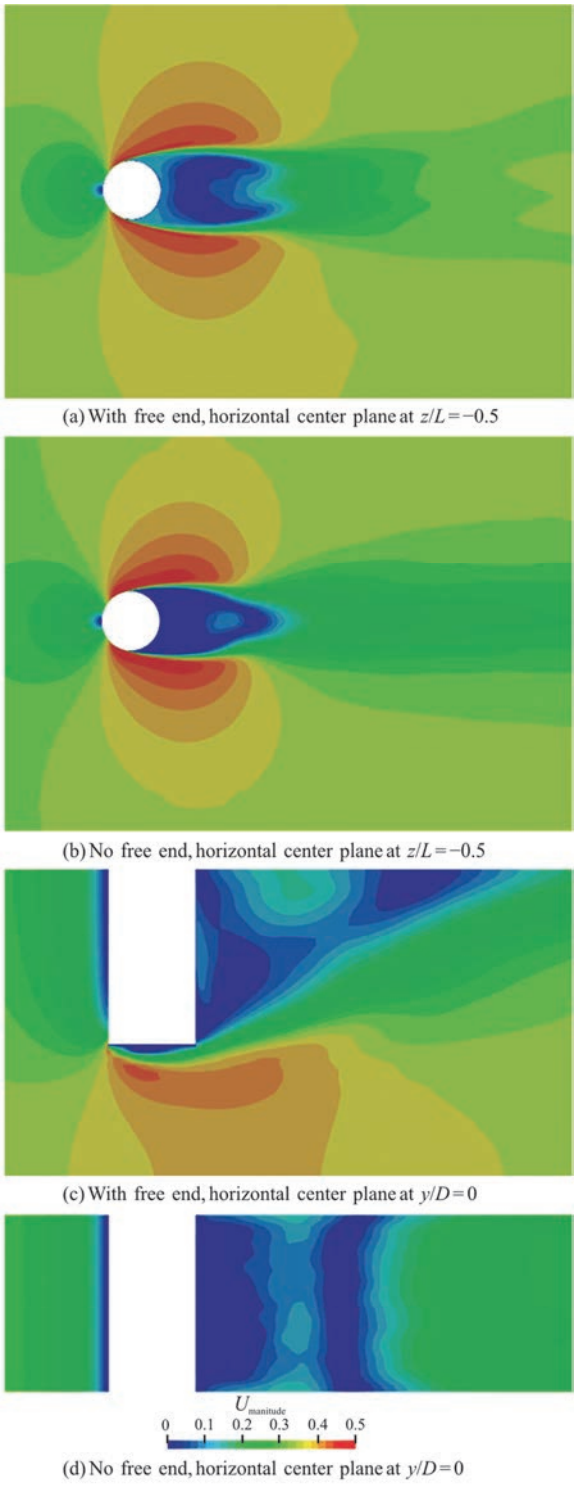

Fig. 5 (Color online) Velocity field near to the fixed cylinder for time $(T=100)$

The free decay results of the computational fluid dynamics (CFD) calculations and the free decay results of experiments by Gonçalves et al.[23] are given in Table 4. The results obtained from the Fourier transform show that the numerical simulation are in good agreement with the experimental results, which further verifies the reliability of the numerical model.

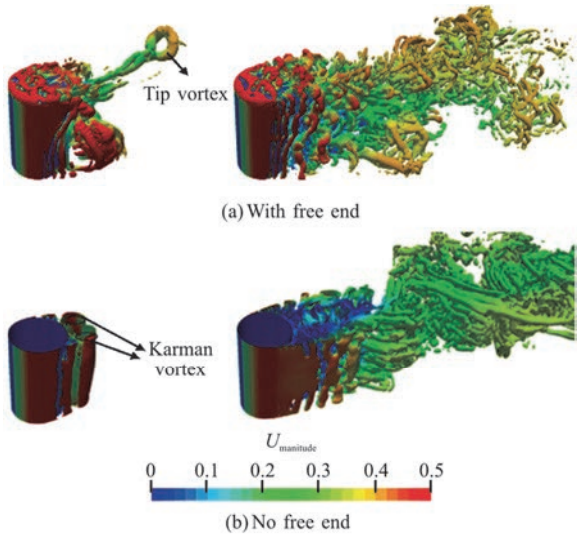

Fig. 6 (Color online) The 3-D vortex contour of flow around fixed cylinder

3.3 *The free end effect of VIM*

The comparison of time history curve for cylinder with or without free end is shown in Fig. 8. It is found that the presence of the free end affects the stability of the in-line motion at low reduced velocities U_r. In this case, below the reduced velocity $U_r = 6$, the amplitude of the in-line motion is unstable and fluctuates greatly up and down. It is possible that the motion is unstable when the energy flow velocity is low, which is closer to the resonant frequency of the transverse motion of the system. With the reduced velocity increase, the amplitude of the transverse motion of the cylinder with free end is more stable, so the motion of the displacement in the crossflow direction is more periodic and more stable in amplitude than in the in-line flow direction.

The motion amplitude of in-line and transverse direction is expressed as dimensionless nominal amplitude which is defined as:

$$\text{Nominal}\quad A_x / D = \frac{\sqrt{2}\sigma[x(t)]}{D} \tag{5}$$

$$\text{Nominal}\quad A_y / D = \frac{\sqrt{2}\sigma[y(t)]}{D} \tag{6}$$

where $x(t)$ is the time histories of the surge motion, $y(t)$ is the time histories of the sway motion. $\sigma[x(t)]$, $\sigma[y(t)]$ is the standard deviation of $x(t)$, $y(t)$ respectively.

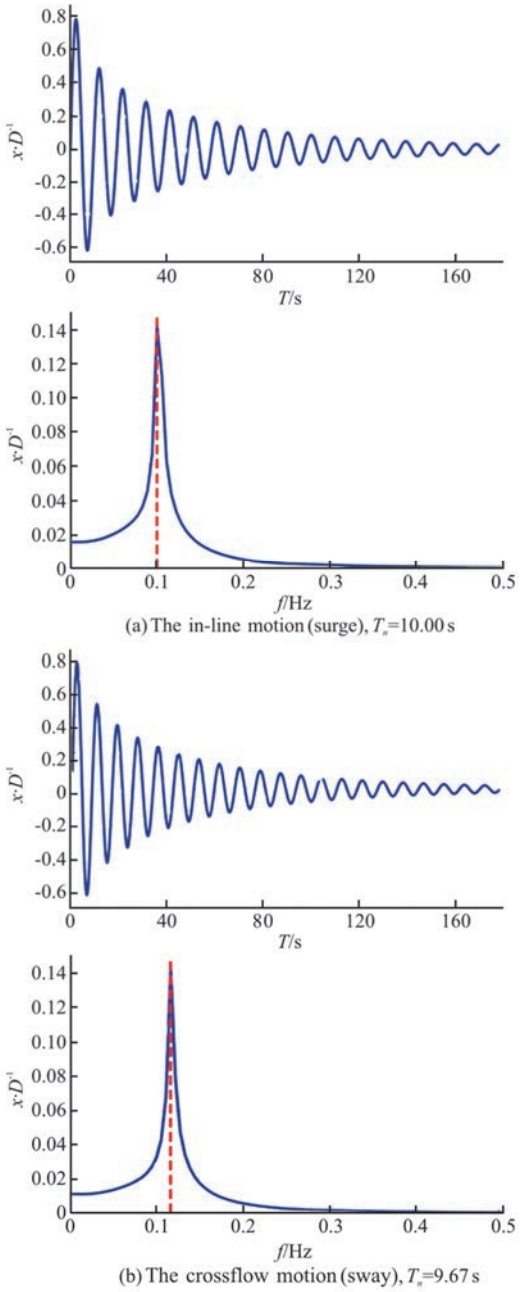

Fig. 7 (Color online) The time evolution of free decay test and its fast Fourier transform results

Table 4 Natural periods from the free decay tests

Item	Exp.	Present	Difference/%
Surges	10	10.01	0.1%
Sways	10	9.67	3.3%

Figure 9 shows the dimensionless nominal motion amplitude in the crossflow and in-line directions for different reduced velocities U_r. The trend in the figure shows that the motion in both directions increases with the increase of incoming current's speed, and the dimensionless nominal amplitude tends to be stable at the reduced velocities of $U_r = 15$. The "lock-in" phenomenon is not observed in both present CFD or experiment by Gonçalves et al.[23]. In the in-line direction, it can be observed that the amplitude of the cylinder will increases as the current velocity increases. What's more, the trends of run up can also be found in the crossflow motion amplitudes. In the crossflow direction, the amplitude increases to 1.4.

In comparison, it is found that the addition of the free end reduces the amplitude of the crossflow direction motion during the numerical simulation, and this free end effect is reduced only when the incoming flow velocity is large. Therefore, we consider that the tip vortex at the free end could suppress the VIM for the single column platform.

Figure 10 demonstrates XY-motion plot trajectories of cylinder with or without free-end at different reduced velocities. It can be observed that the amplitude of the in-line motion of the cylinder will keeps increasing as the increase of reduced velocities U_r. Before the reduced velocities of 6, the transverse displacement has a periodic motion, but its amplitude is not stable, which is related to the failure of the wake field to form a stable vortex shedding. After the reduced velocities of 8, the cylindrical wake field forms a stable vortex shedding, so the transverse and in-line displacements are more periodic and the amplitude is more stable, and the overall trajectory is in the shape of an "8". With the further increase of the reduced velocities, the growth trend of the amplitude of the in-line and crossflow motions slows down and becomes stable at the reduced velocities of about 10. From the trajectory diagram, it can be seen that the amplitude of the in-line motion of the cylinder increases when the incoming velocity increases, regardless of whether it has a free end or not. The overall trajectory of the free-ended cylinder is more stable, with a "c" shape at the beginning and an "8" shape as the reduced velocities increases. The overall trajectory of the VIM without the free-end cylinder is initially in the shape of a "c", and later in a single cycle, a deformation similar to a flattened "8" can be seen, but the regularity of the overall motion is not obvious.

The vortex shedding periods at the in-line and crossflow directions is shown in Table 5. For the cylinder with free ends, it can be seen that the in-line oscillation period T_y of the vortex motion is twice the transverse oscillation period T_x, which explains the relatively regular positive "8" shape of the motion trajectory of the cylinder with free ends. It is also found that the presence of the free end increases the vortex shedding period as a whole, and the vortex shedding period of the column with free end is found to be smaller in the Table 5.

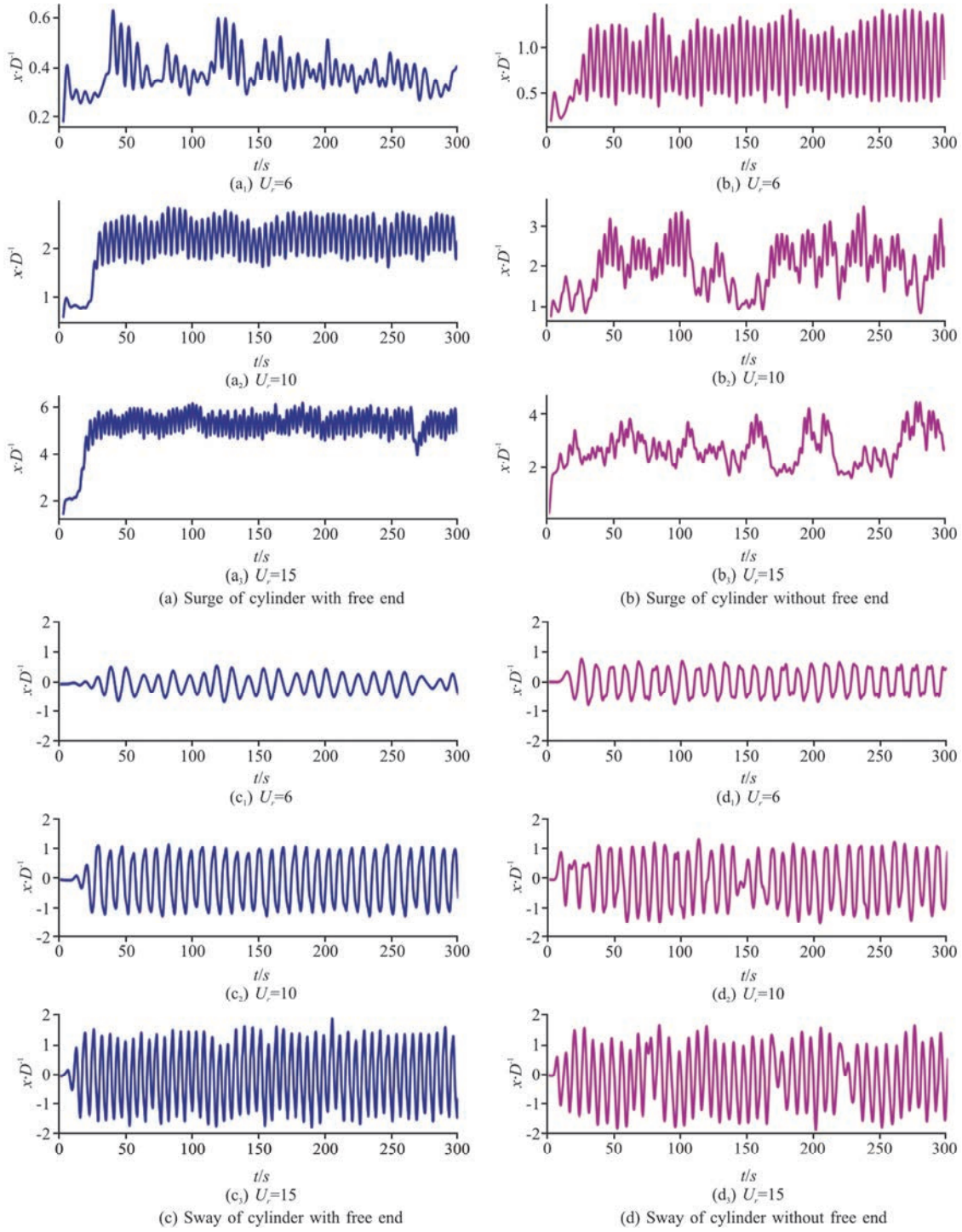

Fig. 8 (Color online) Time history curve of in-line and crossflow direction motion at different reduced velocity

Figure 11 shows a comparison of the Fourier transform of transverse motion time history. At low reduced velocity, the peak of oscillation occurs near the intrinsic frequency of the cylinder (red dashed line in the figure), and the frequency distribution of the motion is concentrated. The motion amplitude does not increase with the increase of the folding speed.

As the reduced velocity increases, the motion frequency of the platform shows a complex frequency characteristic. Comparing Figs. 11(a), 11(b), it can be found that the motion frequency distribution of the platform with free end is more dispersed, and many higher-order frequency components appear near the main frequency. The scattered amplitude-frequency characteristics may be related to the complex wake field distribution, and the analysis may be the presence

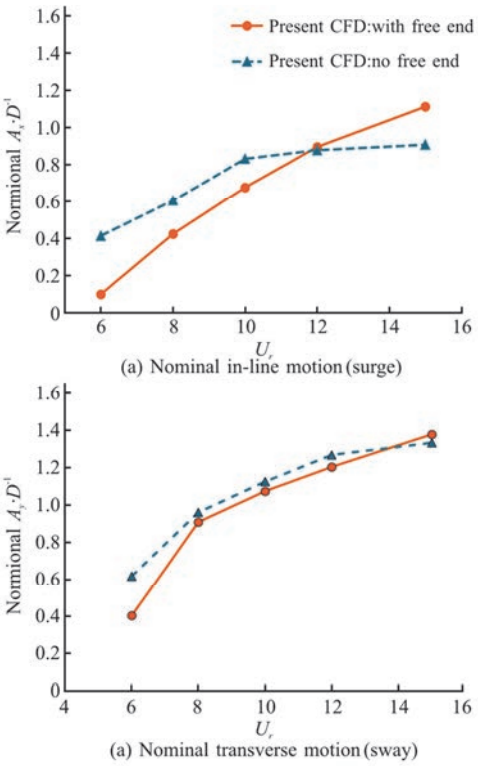

Fig. 9 (Color online) Characteristic motion amplitude of VIM at different reduced velocities

of the tip, which destroys the main frequency of the Karman vortex street. Moreover, for the peak value $S(f)$ of the FFT energy spectrum, it is found that the $S(f)$ of cylinder without free end is larger than that of cylinder with free end case, which further indicates that the tip vortex consumes a lot of vortex shedding energy.

Table 5 Summary of the vortex shedding periods at the in-line and crossflow directions

Reduced velocity, U_r	No free end		With free end	
	T_x /s	T_y /s	T_x /s	T_y /s
$U_r = 6$	5.4	10.7	6.0	11.8
$U_r = 8$	4.3	9.1	5.2	10.4
$U_r = 10$	5.3	8.7	4.3	8.6
$U_r = 12$	5.2	7.4	3.8	7.6
$U_r = 15$	4.8	5.9	3.0	6.0

For the vortex identification, we employ Omega-Liutex criterion[28] to visualize the vortical structures. Figure 12 shows the instantaneous 3-D vortex contour surface using Omega-liutex criterion, $\Omega_{\text{Liutex}} = 0.52$, and the contour surface is colored by velocity magnitude. It can be seen that due to the platform motion, the three-dimensional vortex and the platform motion

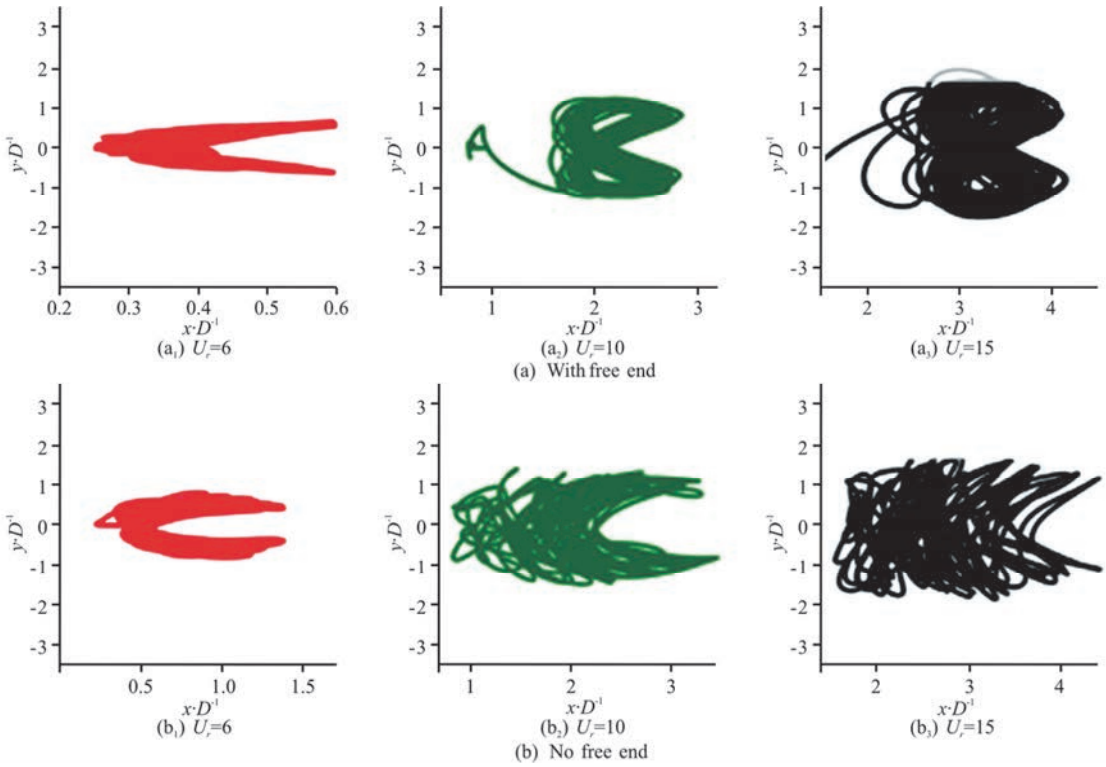

Fig. 10 (Color online) The XY - motion plot trajectory of the cylinder with or without free end

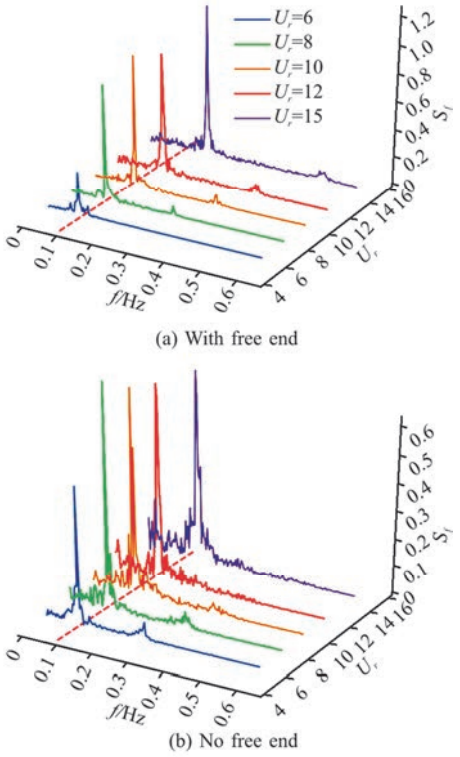

Fig. 11 (Color online) The comparison of the Fourier transform of transverse motion time history

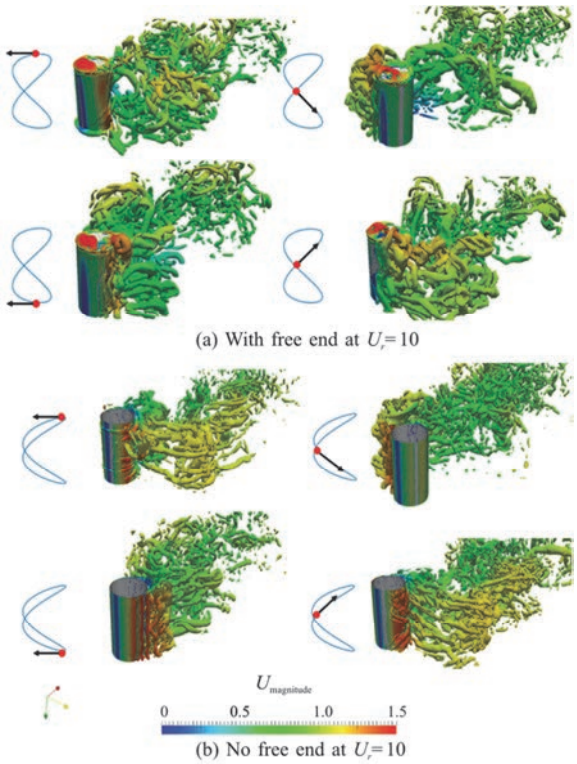

Fig. 12 (Color online) The 3-D vortex contour of cylinder with VIM

interfered with each other and coupled, forming more broken small vortices compared with the case of flow around fixed cylinder. Stronger VIM responses with intensive fluid-structure interaction may strengthen turbulent flow intensity. In addition, due to the presence of the free end, a tip vortex is generated from the end, which dissipates most of the motion energy, and the tip vortex generates a “downwash effect”, forcing the cylindrical vertical shear layer separation is no longer a straight line vertically parallel to the cylindrical axis, but becomes inclined and curved, and the flow separation and vortex sheddiing periodicity is destroyed. It can be considered to suppress the single-column platform VIM by the addition of vortex at the tip of free end.

4. Conclusions

A series of numerical investigations on VIM of a rigid cylinder with free end have been conducted in this paper using the vim-FOAM-SJTU solver. The following key conclusions can be made from this study:

(1) The present CFD calculation results of the VIM amplitude have shown generally good agreement for the model test results. And it is demonstrated that the simulation method and vim-FOAM-SJTU solver can be applied for various kinds of cylindrical floaters in current.

(2) The flow velocity in the near flow field behind the cylinder is larger than that in the far flow field. Overall, for the case of cylinder with free end, the flow velocity is larger than that of cylinder without free end. The length of the wake field zone with the free-ended cylinder is longer than that of cylinder without free end. Then, by analyzing the vortex characteristics of the fixed and VIM cylinders, it is found that the presence of the free end shortens the shear layer length and disrupts the periodicity of the cylindrical axial vortex.

(3) In the numerical simulation of the VIM of the cylinder with free end, when the reduced velocity U_r is low, it is difficult to form a continuous and stable vortex in the wake field, and the crossflow motion response amplitude is unstable and the overall motion trajectory is chaotic. As the reduced velocity U_r increases, the transverse motion of the column with free ends becomes more regular and the amplitude decreases. By comparing the VIM numerical simulation results of cylinder with or without free end, the addition of the free end can reduce the amplitude of the transverse motion, and this free end effect will be reduced only when the incoming flow velocity is higher.

References

[1] Gonçalves R. T., Franzini G. R., Rosetti G. F. Flow around circular cylinders with very low aspect ratio [J]. *Journal of Fluids and Structures*. *Elsevier*, 2015, 54: 122-141.

[2] Igbalajobi A., McClean J. F., Sumner D. et al. The effect of a wake-mounted splitter plate on the flow around a surface-mounted finite-height circular cylinder [J]. *Journal of Fluids and Structures*, 2013, 37: 185-200.

[3] Iungo G. V., Pii L. M., Buresti G. Experimental investigation on the aerodynamic loads and wake flow features of a low aspect-ratio circular cylinder [J]. *Journal of Fluids and Structures*, 2012, 28: 279-291.

[4] Rostamy N., Sumner D., Bergstrom D. J. et al. An Experimental study of the flow above the free ends of surface-mounted bluff bodies [C]. *ASME 2012 Fluids Engineering Division Summer Meeting collocated with the ASME 2012 Heat Transfer Summer Conference*, Rio Grande, Puerto Rico, USA, 2012, 981-990.

[5] Zhao W., Wan D., Sun R. Detached-eddy simulation of flows over a circular cylinder at high Reynolds number [C]. *The Twenty-sixth (2016) International Ocean and Polar Engineering Conference*, Rhodes, Greece, 2016, 1528-1536.

[6] Rostamy N., Sumner D., Bergstrom D. J. J. et al. Instantaneous flow field above the free end of finite-height cylinders and prisms [J]. *International Journal of Heat and Fluid Flow*, 2013, 43: 120-128.

[7] Rosetti G. F., Vaz G., Hoekstra M. et al. CFD calculations for free-surface-piercing low aspect ratio circular cylinder With solution verification and comparison with experiments [C]. *The 32nd International Conference on Ocean, Offshore and Arctic Engineering*, Nantes, France, 2013, 1-15.

[8] Park C. W., Lee S. J. Free end effects on the near wake flow structure behind a finite circular cylinder [J]. *Journal of Wind Engineering and Industrial Aerodynamics*, 2000, 88(2-3): 231-246.

[9] Krajnović S. Flow around a tall finite cylinder explored by large eddy simulation [J]. *Journal of Fluid Mechanics*, 2011, 676: 294-317.

[10] Palau-Salvador G., Stoesser T., Fröhlich J. et al. Large eddy simulations and experiments of flow around finite-height cylinders [J]. *Flow, Turbulence and Combustion*, 2010, 84(2): 239-275.

[11] Afgan I., Moulinec C., Prosser R. et al. Large eddy simulation of turbulent flow for wall mounted cantilever cylinders of aspect ratio 6 and 10 [J]. *International Journal of Heat and Fluid Flow*, 2007, 28(4): 561-574.

[12] Fröhlich J., Rodi W. LES of the flow around a circular cylinder of finite height [J]. *International Journal of Heat and Fluid Flow*. 2004, 25(3): 537-548.

[13] Sumner D., Heseltine J. L. Tip vortex structure for a circular cylinder with a free end [J]. *Journal of Wind Engineering and Industrial Aerodynamics*, 2008, 96: 1185-1196.

[14] Park H., Ajith Kumar R., Bernitsas M. M. Suppression of vortex-induced vibrations of rigid circular cylinder on springs by localized surface roughness at $3\times10^4 \le Re \le 1.2\times10^5$ [J]. *Ocean Engineering*. 2016, 111: 218- 233.

[15] Fujiwara T. VIM simulation on a cylindrical floating structure [J]. *Journal of Marine Science and Technology*, 2018, 23(2): 288-301.

[16] Morse T. L., Govardhan R. N., Williamson C. H. K. The effect of end conditions on the vortex-induced vibration of cylinders [J]. *Journal of Fluids and Structures*, 2008, 24(8): 1227-1239.

[17] Xu W. H., Wu Y. X., Zeng X. H. et al. A new wake oscillator model for predicting vortex induced vibration of a circular cylinder [J]. *Journal of Hydrodynamics*, 2010, 22(3): 381-386.

[18] Kang Z., Ni W., Zhang L. et al. An experimental study on vortex induced motion of a tethered cylinder in uniform flow [J]. *Ocean Engineering*, 2017, 142: 259-267.

[19] Hirabayashi S. Numerical analysis of vortex-induced motion of two-dimensional circular cylinder by lattice Boltzmann method [J]. *Journal of Marine Science and Technology*, 2016, 21(3): 426-433.

[20] Duranay A., Kinaci O. K. Enhancing two-dimensional computational approach for vortex-induced vibrations by scaling lift force [J]. *Ocean Engineering*, 2020, 217: 107620.

[21] Zhao W., Zou L., Wan D. et al. Numerical investigation of vortex-induced motions of a paired-column semi-submersible in currents [J]. *Ocean Engineering*, 2018, 164: 272-283.

[22] Gritskevich M. S., Garbaruk A. V., Schütze J. et al. Development of DDES and IDDES formulations for the k-ω shear stress transport model [J]. *Flow, Turbulence and Combustion*, 2012, 88(3): 431-449.

[23] Gonçalves R. T., Meneghini J. R., Fujarra A. L. C. Vortex-induced vibration of floating circular cylinders with very low aspect ratio [J]. *Ocean Engineering*, 2018, 154: 234-251.

[24] Liu M., Xiao L., Yang J. et al. Parametric study on the vortex-induced motions of semi-submersibles: Effect of rounded ratios of the column and pontoon [J]. *Physics of Fluids*, 2017, 29(5): 055101.

[25] Gonçalves R. T., Fujarra A. L. C. Experimental study on vortex-induced vibration of floating circular cylinders with low aspect ratio [C]. *ASME 2018 37th International Conference on Ocean, Offshore and Arctic Eiginerring*, Madrd, Spain, 2014.

[26] Rosetti G. F., Vaz G., Hoekstra M. et al. CFD Calculations for free-surface-piercing low aspect ratio circular cylinder with solution verification and comparison with experiments [C]. *The 32nd International Conference on Ocean, Offshore and Arctic Engineering*, Nantes, France, 2013, 1-15.

[27] Schlichting H., Shapiro A. Boundary layer theory [M]. Ninth Edition, Berlin Heidelberg, Germany: Springer-Verlag, 2000.

[28] Charkrit S., Shrestha P., Liu C. Liutex core line and POD analysis on hairpin vortex formation in natural flow transition [J]. *Journal of Hydrodynamics*, 2020, 32(6): 1109-1121.